BMC Genomics

RESEARCH

Open Access

Physiological, ionomic, transcriptomic and metabolomic analyses reveal molecular mechanisms of root adaption to salt stress in water spinach

Zhenqin Li[1], Long Cheng[1], Sitong Li[1], Guangcai Liu[2], Sijia Liu[1], Duo Xu[1], Rongchao Yang[1], Feng Feng[1], Junning Wang[1*] and Chao Zheng[1,3*]

Abstract

Water spinach (*Ipomoea aquatica* Forsk.) is an important leaf vegetable affected by salt stress, however, little is known about its salt adaption mechanism. Here, we integrated physiomics, ionomics, transcriptomics, and metabolomics to analyze the root adaptation response of two water spinach varieties, BG (salt-tolerant) and MF (salt-sensitive), at 150 mM NaCl. The results showed that compared with MF, BG significantly reduced the content of malondialdehyde (MDA) and H_2O_2, and increased catalase (CAT) activity and proline content. Ionome analysis demonstrated that BG significantly reduced Na^+ accumulation and increased K^+ level to reduce the toxicity of Na^+, compared to MF. Weighted gene co-expression network analysis (WGCNA) revealed that key transcription factors such as *HSFA4A*, *bHLH093*, and *IDD7*, which were only up-regulated in BG. Multi-omics revealed that BG reprogrammed key pathways: starch and sucrose metabolism, as well as galactose metabolism, leading to decreased amylose production and increased sucrose and galactose levels, helping to maintain cellular osmotic balance in response to salt stress. These findings provide insight into transcriptional regulation in response to salt stress, which could advance the genetic enhancement of water spinach.

Highlights

- BG had stronger osmotic regulation ability and ROS scavenging capacity.
- BG elevated expression of Na^+ efflux and K^+ transporter genes decreased Na^+ toxicity and balanced Na^+/K^+ homeostasis.
- Starch and sucrose metabolism and galactose metabolism were the key metabolic pathways in the salt tolerance in BG.
- Increased sucrose and stachyose enhanced the salt resistance in BG.

*Correspondence:
Junning Wang
wangjunningb@126.com
Chao Zheng
zhengchao@gdou.edu.cn

Full list of author information is available at the end of the article

Keywords Water spinach (*Ipomoea aquatica* Forsk.), Salt stress, Seedling stage, Na^+ content, Transcriptome and metabolome

Introduction

Worldwide, over 20% of agricultural land, which amounts to 10 billion hectares, is impacted by salinity [1]. This figure is increasing as a result of climate change and poor irrigation and fertilizer management [2, 3]. Soil salinity is a primary abiotic stress factor that hinders plant growth and development, leading to decreased crop yields and significant economic losses [4–6] In saline soils, plants experience osmotic stress, oxidative stress, and ionic stress [7]. Plants respond to oxidative stress caused by salt stress by increasing the activity of oxidases, scavenging reactive oxygen species (ROS), such as peroxidase (POD), ascorbate peroxidase (APX), and CAT [8]. Maintaining Na^+/K^+ balance and accumulating osmoprotective agents are common strategies for survival under ionic and osmotic stress in plants [9, 10], and the common osmoprotective agents are proline and soluble sugar [11]. In addition, studies have shown that starch and sucrose metabolism are also involved in salt stress adaptation in plants [12]. Starch is catalyzed by β-amylase (BAM), and the sugars and some derived metabolites released by it act as osmoprotective agents and compatible solutes to reduce osmotic stress [13], and also participate in sugar signal transduction as signaling molecules, such as sucrose (Suc) itself, glucose (Glc), fructose (Fru), and trehalose-6 phosphate (T6P) [14, 15]. Sugars, when used as signaling molecules, also interact with auxin signaling pathways and activate downstream signaling pathway [16] The findings demonstrated that the salt stress response mechanism is coordinately modulated by an array of signaling molecules, encompassing phytohormones, with auxin emerging as a pivotal regulator in this intricate network [17]. Under salt stress conditions, pronounced alterations in plant growth and development were observed, underscoring the critical physiological role of auxin in this adaptive process [18]. Notably, an antagonistic interplay was identified between auxin-mediated lateral root development and its growth-inhibitory effects elicited under high salinity conditions [19]. In addition, salicylic acid (SA) can improve plant salt tolerance by enhancing the antioxidant system and the synthesis of osmotic substances and promoting photosynthesis in plants [20].

With the widespread use of various omics, multiomics has also been used to study the tolerance mechanism of plants to salt stress. A multi-omics approach can provide insight into different levels in order to better understand the complex molecular network behind plant abiotic tolerance mechanisms [21, 22]. For example, integrative transcriptomics and metabolomics revealed that glutathione metabolism plays a crucial role in tomato salt stress adaptation [23]. In addition, it is also used in a variety of crops, such as oats [24], soybeans [25], peppers [26], etc.

Water spinach (*Ipomoea aquatica* Forsk.), adaptable to grow both in water and soil, is a key vegetable in Southeast Asia, China, and India [27–29]. By 2023, following the initial genome assembly of water spinach in 2021 [30], notable enhancements to the genome were realized [31], facilitating transcriptome sequencing. Water spinach is a glycophyte crop [32]. There are in-depth studies on the salt tolerance of water spinach, mainly at the physiological and transcriptional levels. However, there are few studies on the combined analysis of metabolomics and transcriptomics of water spinach under salt stress. In this study, we selected 2 cultivars of water spinach, BG (salt-tolerant) and MF (salt-sensitive), from a total of 59 cultivars based on their salt tolerance. A thorough comparison and systematic analysis of the root of both salt-tolerant and salt-sensitive genotypes under salt stress were conducted using the combination of physiological, ionomic, transcriptomic, and metabolomic. The results of this study aimed to provide important insights for improving salt resistance in water spinach and to lay a strong groundwork for future vegetable enhancement initiatives.

Results

Comprehensive salt-tolerance evaluations of 59 water spinach cultivars

Based on a correlation analysis (Table S3), 19 relative traits showed a distinct degree of correlation with each other. Therefore, principal component analysis (PCA) was performed on 19 relative traits, and they were transformed into 4 independent principal components based on a cumulative contribution rate of more than 80% (Table S4). Salt tolerance comprehensive evaluation analysis classified 59 water spinach species into 3 groups, i.e., salt-tolerant, medium salt-tolerant, and salt-sensitive (Table S5).

Morphological traits and physiological indicators in two varieties

Based on salt-tolerant germplasm screening studies in water spinach, we selected salt-tolerant cultivar BG and salt-sensitive cultivar MF (Fig. 1A and Table S5). After 7 days of salt stress, typical symptoms in MF, such as yellow, brown, and curly leaves, were observed, while the leaves in BG remained unchanged (Fig. 1A). Compared to the control group (CK), the root system in MF was

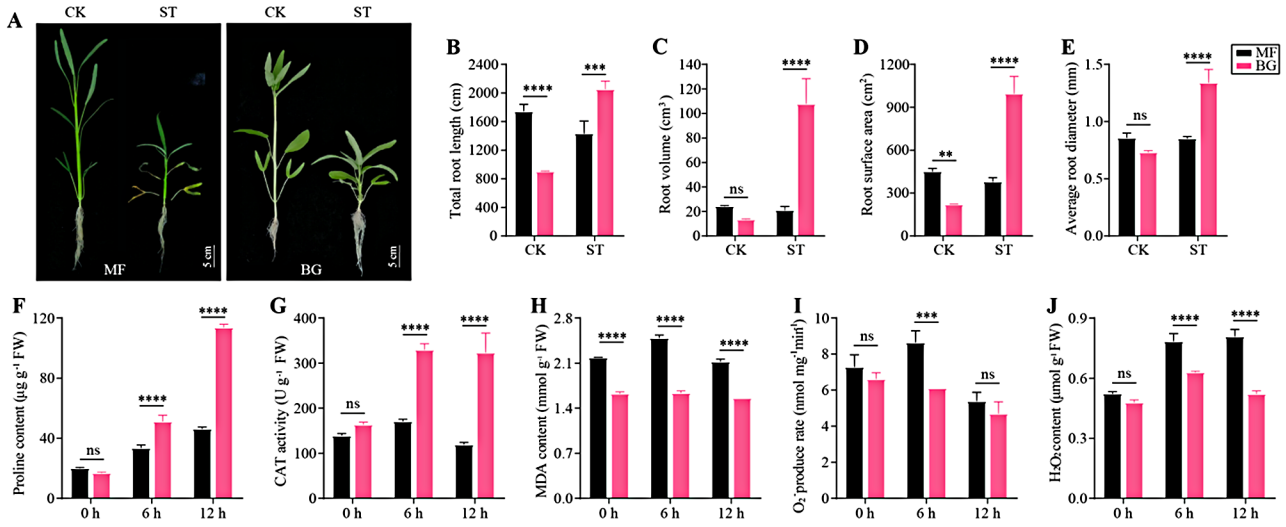

Fig. 1 Morphological changes and physiological responses MF (salt susceptible) and BG (salt tolerant) under salt stress. (**A**) Morphological traits in MF and BG, (**B**) Total root length (cm), (**C**) Root volume (cm^3), (**D**) Root surface area (cm^2), (**E**) Average root diameter (mm), (**F**) Proline content (μg g^{-1} FW), (**G**) CAT activity (U g^{-1} FW), (**H**) MDA content (mmol g^{-1} FW), (**I**) O_2•$^-$ production rate (nmol g^{-1} min^{-1}), (**J**) H_2O_2 content (μmol g^{-1} FW). Vertical bars indicate the mean standard error. Ns indicates no significant difference, and ** and **** indicate significant differences between MF and BG at $P < 0.01$ and $P < 0.001$ by the One-Way ANOVA test

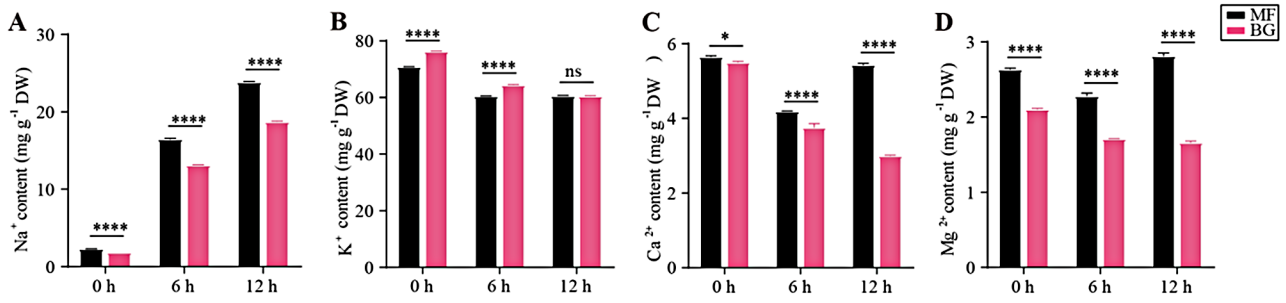

Fig. 2 Contents of Na^+ (**A**), K^+ (**B**), Ca^{2+} (**C**), and Mg^{2+} (**D**) were determined in the roots of MF and BG after 0, 6, 12 h salt treatments. Vertical bars indicate the mean standard error. Ns indicates no significant difference, and * and **** indicate significant differences between MF and BG at $P < 0.05$ and $P < 0.001$ by the One-Way ANOVA test

significantly weaker, while the root system of BG was stronger. Root phenotypic analysis revealed that the total root length (TRL), root volume (RV), root surface area (RSA), and average root diameter (ARD) in MF were significantly lower than those in BG (Fig. 1B-E). Additionally, a physiology analysis of water spinach roots under salt stress was performed. The proline content increased slowly in MF but sharply in BG, with BG showing significantly higher proline levels (Fig. 1F). The activity of CAT in BG sharply increased and remained significantly higher than in MF (Fig. 1G), and the activity of POD, APX, and glutathione reductase (GR) increased upon salinity condition in both cultivars (Fig. S1A–C). The MDA content decreased in BG and was notably lower than in MF under salt stress (Fig. 1H). The superoxide anion (O_2•$^-$) production rate was significantly higher in MF compared to BG at 6 h after salt stress (Fig. 1I). The H_2O_2 content continued to increase in MF, while in BG it increased slowly and then decreased, with BG showing significantly lower H_2O_2 levels than MF (Fig. 1J).

Ion level changes in two varieties

An ion dynamics analysis in water spinach roots under salt stress revealed interesting patterns of Na^+, K^+, Ca^{2+}, and Mg^{2+} levels. At 6 and 12 h post-salt exposure, a significant increase in Na^+ ion levels occurred in the roots of both varieties. However, BG demonstrated superior efficacy in managing Na^+ concentrations, keeping significantly lower levels of Na^+ compared to MF (Fig. 2A). Conversely, K^+ levels decreased significantly in both MF and BG, with BG exhibiting higher K^+ content compared to MF at 6 h under salt stress (Fig. 2B). The levels of Ca^{2+} and Mg^{2+} showed similar trends, decreasing in BG but initially decreasing and then increasing in MF. Despite these alterations, Ca^{2+} and Mg^{2+} concentrations remained significantly elevated in MF as opposed to BG,

with the Ca^{2+} levels in MF registering at 1.82 times the amount observed in BG at 12 h of salt stress (Fig. 2C and D).

Comparing transcriptome analysis in two varieties

Transcriptome sequencing was conducted on a total of 18 root samples (2 cultivars, 3 treatments, and 3 biological replicates). A total of 123.03 Gb of clean data was generated with an average of 6.84 Gb of clean data for each sample. The Q30 base percentage exceeded 96.85% (Table S6). In the PCA, the first principal component (PC1) and the second principal component (PC2) explained 36.3% and 20.4% of the variation (Fig. 3A). The samples were separated based on salt treatment time along PC1 and by water spinach cultivars along PC2. Correlation analysis uncovered that the correlations between the 3 replicates were 1, showing the reliability of sequencing data (Fig. 3B).

To identify DEGs, pairwise comparisons were conducted, including MF0 vs. MF6, MF0 vs. MF12, MF6 vs. MF12, BG0 vs. BG6, BG0 vs. BG12, and BG6 vs. BG12. Among these comparisons, more DEGs were found in BG (Fig. 3C), suggesting that the response of gene expression to salt stress was more pronounced in BG. Based on the overall number of DEGs, MF0 vs. MF6 and BG0 vs. BG6 comparisons were focused on for further analysis. A Venn diagram illustrated that 4,096 DEGs were shared between MF and BG, while 1,106 and 1,946 DEGs were unique to MF and BG respectively (Fig. 3D).

KEGG analyses were conducted on the 4,096 common DEGs (Fig. 3E). KEGG analysis revealed significant enrichment in the biosynthesis of secondary metabolites (ko01110), metabolic pathways (ko01100), starch and sucrose metabolism (ko00500), and phenylpropanoid biosynthesis (ko00940) (Fig. 3E). Furthermore, KEGG analyses were performed on the unique DEGs in MF and BG (Fig. S2). In the KEGG analysis, unique genes

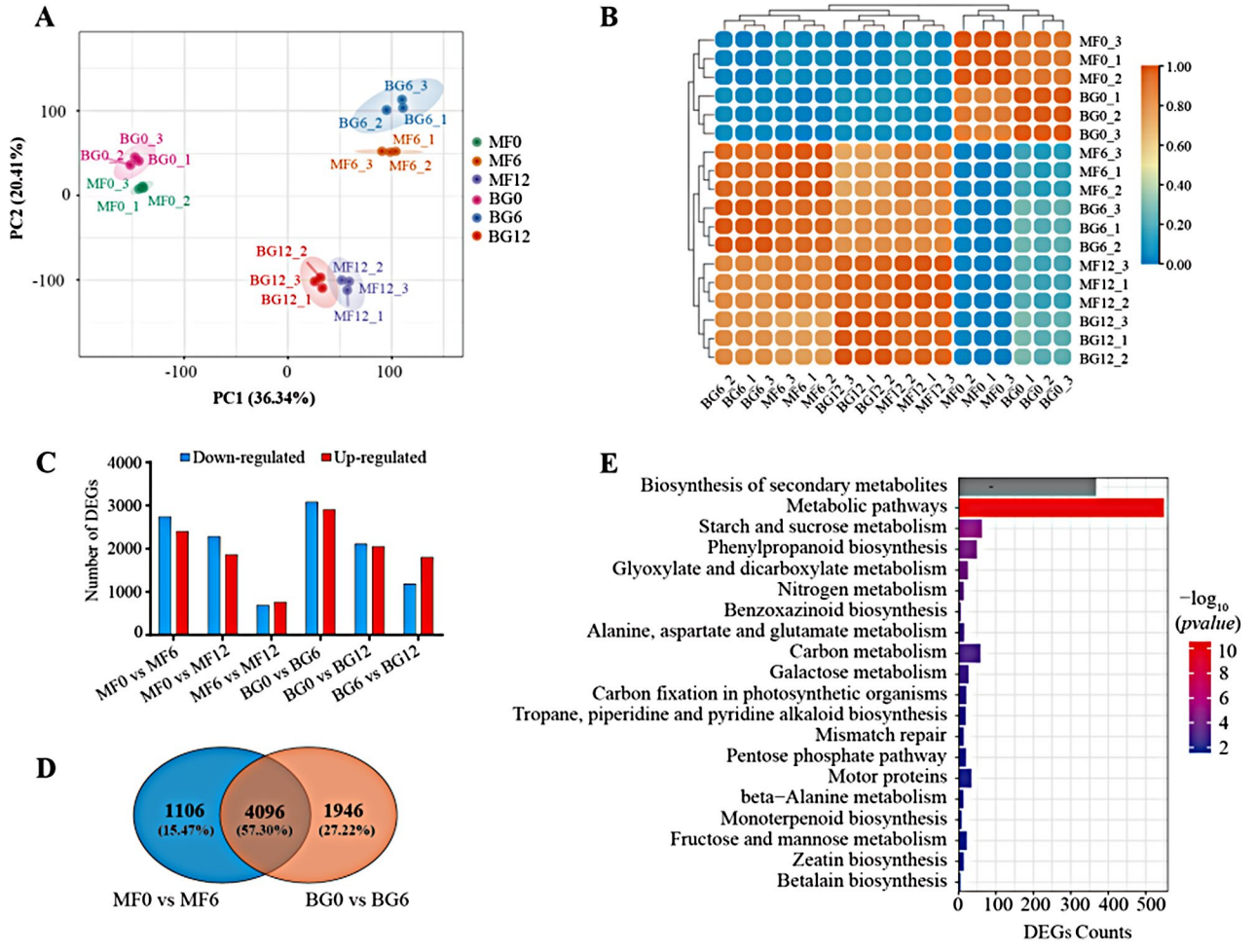

Fig. 3 Transcriptome analysis of MF and BG under salt stress. (**A**) PCA of 18 samples, (**B**) Correlation analysis of 18 samples, (**C**) The numbers of DEGs in the different comparison groups, (**D**) Venn analysis of DEGs in MF0 vs. MF6 and BG0 vs. BG6: MF0 samples at 0 h, MF6 samples at 6 h, BG0 samples at 0 h, BG6 samples at 6 h. (**E**) KEGG analysis of 4096 common DEGs

in MF were significantly enriched in flavonoid biosynthesis (ko00941) and glutathione metabolism (ko00480) (Fig. S2A), while unique genes in BG were remarkably enriched in plant hormone signal transduction (ko04075), phenylpropanoid biosynthesis (ko00940), and MAPK signaling pathway (ko04016) (Fig. S2B).

Ion transportation in two varieties

In the comparisons MF0 vs. MF6 and BG0 vs. BG6, a total of 53 DEGs were identified, which predominantly included 4 Na^+ transporters, 18 K^+ transporters, and 21 Ca^{2+} transporters (Table S7). These genes exhibited expression patterns under salt stress (Fig. 4). Specifically, about Na^+ transporters, *NXH6* (*Iaqu.ptg000021l.g503*) and *HKT1:3* (*Iaqu.ptg000014l.g986*) were induced in 2 cultivars. Concerning K^+ transporters, *SKOR* (*Iaqu.ptg000031l.g490*) showed induction at 6 h post-salt stress, with higher expression levels observed in BG. *ILK1* (*Iaqu.ptg000017l.g126*) exhibited up-regulation in BG but down-regulation in MF. Among the 4 *TOP* genes that were upregulated, *TOP2* (*Iaqu.ptg000023l.g792*) displayed higher expression levels in BG. Notably, *TOP5* (*Iaqu.ptg000008l.g837*) was upregulated in MF but down-regulated in BG under salt stress. In terms of Ca^{2+} transporters, 9 genes were induced at 6 h under salt stress, with higher expression levels observed in BG, such as *CNGC1* (*Iaqu.ptg000017l.g24*), *CALM1* (*Iaqu.ptg000004l.g511*), *CML2* (*Iaqu.ptg000011l.g1598*), and *CML48* (*Iaqu.ptg000006l.g705*). Conversely, *CML25* (*Iaqu.ptg000026l.g71*) and *CML39* (*Iaqu.ptg000006l.g770*) were up-regulated in BG but down-regulated in MF. Additionally, regarding Mg^{2+} transporters, *MRS23* (*Iaqu.ptg000011l.g230*) was induced in 2 cultivars. Furthermore, 8 DEGs involved in transporting Na^+, K^+, Ca^{2+}, and Mg^{2+} displayed distinct expression patterns. For instance, *CIPK24* (*Iaqu.ptg000014l.g803*), *NAKR1* (*Iaqu.ptg000018l.g662*), *TSC10A* (*Iaqu.ptg000008l.g1159*), and *MYB36* (*Iaqu.ptg000020l.g12600*) showed up-regulation, with *NAKR1*, *TSC10A*, and *MYB36* demonstrating higher expression levels in BG (Fig. 4).

Hormone signaling in two varieties

We identified 39 DEGs related to hormone signaling in water spinach under salinity stress (Table S8), and their expression patterns were analyzed (Fig. 5). In ABA signaling, *ABI1* (*Iaqu.ptg000001l.g1089*) and *PYL3* (*Iaqu.ptg000017l.g28*) transcripts exhibited a significant increase with 7.9-fold and 9.2-fold in BG, but 3.8-fold and 5.7-fold in MF under salinity conditions respectively (Fig. 5). Moreover, 4 genes related to SA signaling exhibited a higher degree of up-regulation in BG, such as two *TGA* genes (*Iaqu.ptg000012l.g994* and *Iaqu.ptg000024l.g210*) and two *PR1* genes (*Iaqu.ptg000011l.g241* and *Iaqu.ptg000014l.g1106*) (Fig. 5).

Construction and analysis of the weighted gene co-expression networks

DEGs in MF and BG were examined through WGCNA, utilizing physiological indicators as the trait file (Fig. 1 and 2). 16 modules were generated, with the turquoise module (5571) having the highest number of DEGs, whereas the midnightblue module (95) had the smallest amount (Fig. 6A and S3). Out of the 16 modules, the black module showed a significant correlation with CAT,

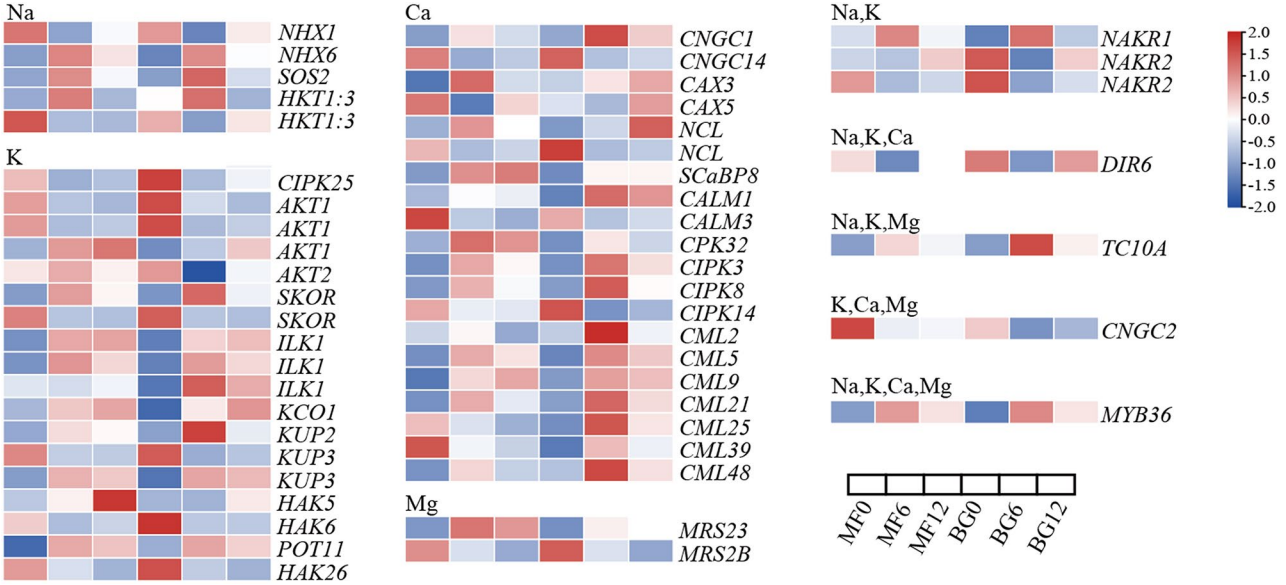

Fig. 4 The DEGs expression piles of Na^+, K^+, Ca^{2+}, and Mg^{2+} transporters in MF and BG under 0, 6, and 12 h salt treatments

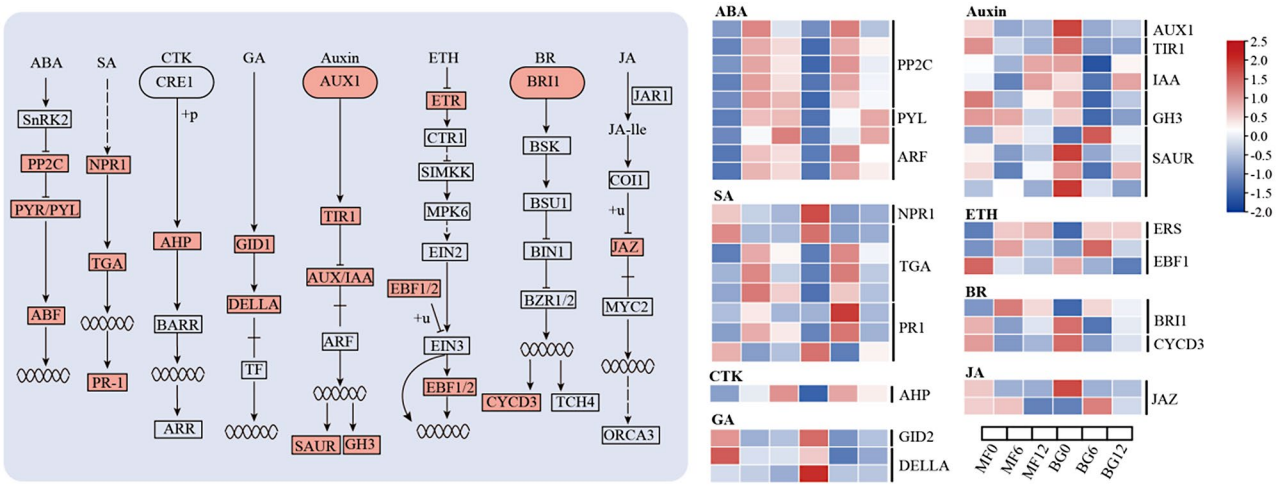

Fig. 5 The DEGs expression piles of hormone signaling in MF and BG under 0, 6, and 12 h salt treatments. PP2C, protein phosphatase 2 C; PYL, pyrabactin resistance; ARF, Auxin response factor; NPR1,nonexpressor of pathogenesis-related genes 1; PR1, pathogenesis related protein 1; AHP, histidine-containing phosphotransmitters; AUX1, AUXIN1; IAA, auxin/indole-3-acetic acid; SAUR, small auxin-up RNA; ERS, endoplasmic reticulum stress; BRI1, brassinosteroid Insensitive 1; CYCD3, D-type cyclins 3; JAZ, jasmonate ZIM-domain

MDA, and Ca^{2+}, while the cyan module had a notable correlation with proline and $O_2\bullet^-$. The black module contained 725 genes that were significantly associated with CAT (correlation coefficient of 0.86), MDA (-0.91). Similarly, the blue module included 143 genes that had a significant relationship with proline (0.89) and $O_2\bullet^-$ (-0.83). The DEGs in the black and cyan modules exhibited increased expression levels under salt stress in BG (Fig. 6B), especially at 12 h. Genes from both modules were chosen for further investigation.

Additionally, a total of 23 and 2 transcript factor (TF) genes were in blue and cyan module respectively (Table S9). A co-expression network between TF genes and other genes was constructed based on their expression correlation coefficient over 0.9 (Fig. 11). Within the black module, 23 TFs were found to interact with 113 structural genes, exhibiting varying quantities and degrees of interactions. Notably, *bHLH93* (*Iaqu.ptg000005l.g441*) displayed interactions with 32 genes, followed by *HSFA4A* (Iaqu.*ptg000002l.g582*) with 31 genes, *IDD7* (*Iaqu.ptg000004l.g1874*) with 23 genes, *MYB306* (*Iaqu.ptg000007l.g716*) with 20 genes, and *NAC82* (*Iaqu.ptg000018l.g1481*) with 3 genes. Additionally, *bHLH93* demonstrated strong interactions with *U74E2*, *PCR2*, and *ERCC1*; *HSFA4A* strongly interacted with *LTP4.1*, *CIPK25*, and *SCP17*; *IDD7* exhibited strong interactions with *UVR8*, *PPA1*, and *EF2*; *MYB306* displayed strong interactions with *CUAOZ*, *VAP42*, and *PCR2*; while *NAC82* had a strong interaction with *CAMT*. In the cyan module, *WLIM1* (*Iaqu.ptg000003l.g1237*) and *ANL2* (*Iaqu.ptg000022l*.g452) transcript factors were found to interact with 12 and 3 structural genes respectively. Specifically, *WLIM1* exhibited strong interactions with *PBL10*, *PGLR2*, and *LOX11*, while *ANL2* strongly interacted with *PGLR2*.

Metabolomic response of water spinach roots under salt stress

A total of 4,243 metabolites were identified in root samples, categorized into 21 classes (Fig. 7A). The most prevalent were amino acids and their derivatives, comprising 1,334 metabolites, followed by organic acids with 495. To improve the reliability of the experimental data and findings, three repetitions were conducted for each group. In the PCA, PC1 and PC2 accounted for 30.95% and 19.71% of the variation, respectively. PC1 distinguished the 18 samples based on variety, while PC2 differentiated them by treatment (Fig. 7B). Hierarchical cluster analysis (HCA) indicated that the samples from the same cultivar grouped together, while samples collected at different times from both cultivars were separated (Fig. 7C).

In the MF analysis, 663 differentially abundant metabolites (DAMs) were identified, with 361 being up-regulated and 361 down-regulated, when comparing MF0 to MF6, and 572 DAMs were found in the comparison of MF0 to MF12, consisting of 283 up-regulated and 289 down-regulated metabolites (Fig. 8A). For the BG analysis, 575 DAMs were identified between BG0 and BG6, with 302 up-regulated and 273 down-regulated, and 611 DAMs were found between BG0 and BG12, including 260 up-regulated and 351 down-regulated (Fig. 8B). K-MEAN analysis categorized a total of 2060 DAMs into five subclasses (Fig. 8C). Subclass 5 had the highest number of metabolites (543), while subclass 3 had the fewest (241). Aside from subclass 5, the metabolites in both species exhibited similar patterns in the other subclasses. In both cultivars, the up-regulated metabolites at 6 and 12 h

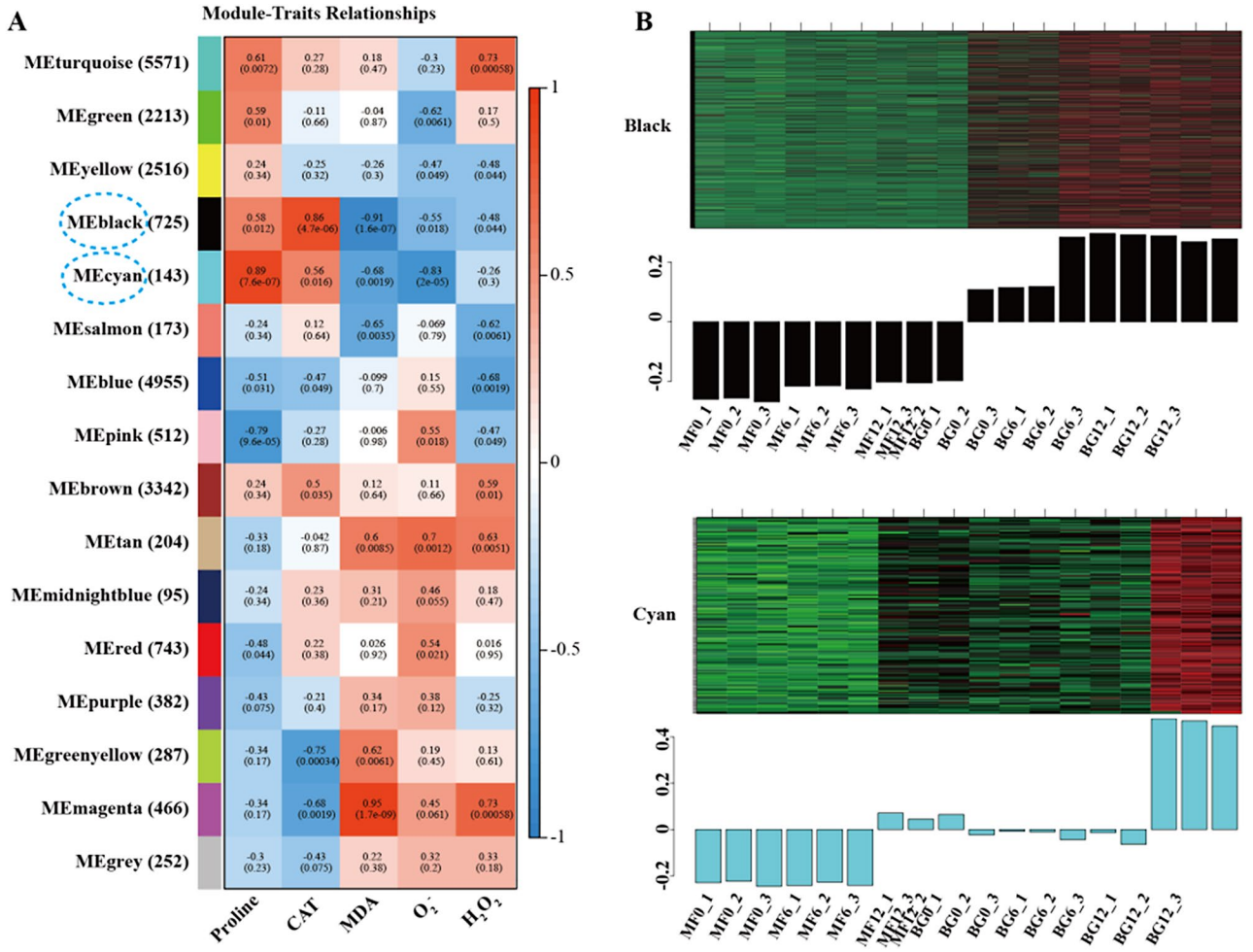

Fig. 6 Identification of gene networks involved in enhanced salt tolerance in water spinach. (**A**) Relationship among co-expression modules and physiological indicators. Heatmap showing correlations between co-expression modules (vertical axis) and traits (horizontal axis). Blue colors indicate negative correlations, and red values indicate positive correlations. *P*-values are shown inside paentheses. (**B**) Gene expression profile for the black and cyan module in different samples. The heat map above shows the expression profiles of all co-expressed genes, and the bar graph below shows the expression patterns of co-expressed genes

primarily included amino acids and their derivatives, organic acids, and flavonoids at 12 h (Table S10). Venn analysis indicated that there were 417 DAMs unique to MF, 329 unique to BG, and 246 shared between MF and BG from 0 to 6 h (Fig. 8D). A heat map cluster analysis of the 246 shared DAMs revealed two distinct groups (Fig. 8E). Group I, which included 137 metabolites, showed an increase in content during salt stress in both cultivars, primarily consisting of amino acids and derivatives, as well as organic acids. In contrast, Group II contained 109 metabolites that decreased in content during salt stress, with the main metabolites being amino acids, derivatives, and GP.

Integrative transcriptome and metabolome analysis under salt stress

Log_2-converted data for DEGs and DAMs were chosen based on a Pearson's correlation coefficient (PCC) more than 0.8. Nine quadrant diagrams were created to illustrate the changes in DAMs and their related DEGs in response to salt stress (Fig. S4). These diagrams displayed unchanged DAMs alongside up-regulated or down-regulated DEGs and unchanged DEGs with upregulated or downregulated DAMs in quadrants 2, 4, 6, and 8. As depicted in Figure S4, quadrant 3 contained 2,381 DEGs linked to 269 DAMs in the comparison of MF0 vs. MF6, and 2,868 DEGs associated with 268 DAMs in the comparison of BG0 vs. BG6. In quadrant 2,572 DEGs corresponded to 309 DAMs in MF0 vs. MF6, and 2,888 DEGs linked to 247 DAMs in BG0 vs. BG6.

The DEGs and DAMs in the comparisons of MF0 vs. MF6 and BG0 vs. BG6 were collectively enriched in various KEGG pathways (Fig. S6 and Table S11 and S12). A total of 70 KEGG pathways were identified for both MF and BG, with 45 pathways common to both cultivars, 11 pathways exclusive to BG, and 14 pathways unique to MF

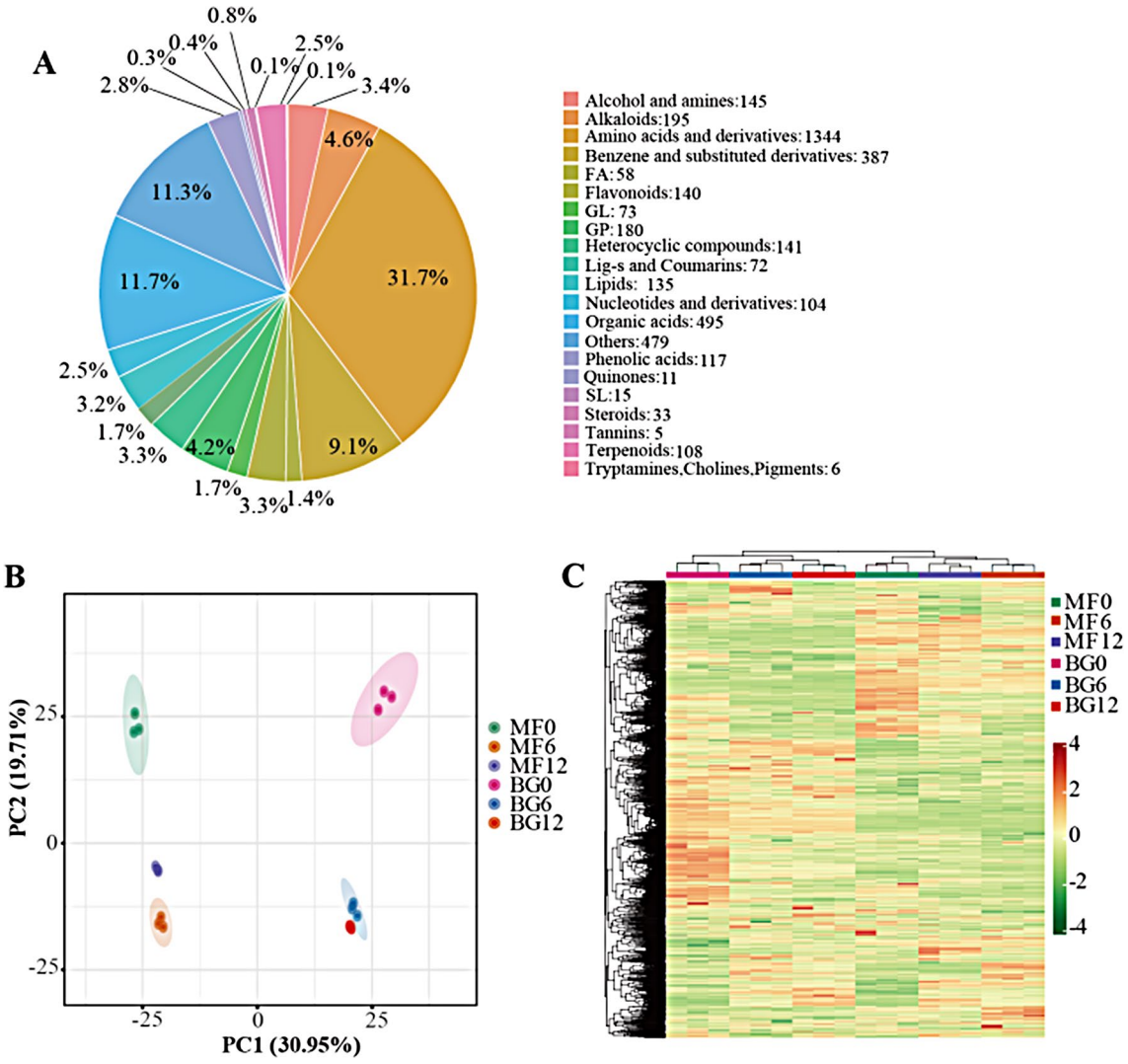

Fig. 7 The metabolites identified in water spinach roots under salt stress. (**A**) PCA of the metabolites. (**B**) Hierarchical cluster analysis of metabolites in 18 samples. (**C**) Hierarchical cluster analysis

(Table S13). Among the KEGG pathways that were significantly annotated ($P < 0.05$) in at least one omics dataset from MF and BG, a total of 11 pathways were shared by both cultivars, mainly related to the synthesis and metabolism of carbohydrates, amino acids, and flavonoids. Furthermore, MF had 5 unique pathways, including cutin, suberine, wax biosynthesis, tryptophan metabolism, and the pentose phosphate pathway. BG had 8 unique pathways, such as starch and sucrose metabolism, galactose metabolism, and carotenoid biosynthesis (Fig. S5). The integrated analysis revealed notable differences in how the two cultivars respond to salt stress, with sugar metabolism being a crucial factor in this response.

The transcription and metabolin difference in starch and sucrose metabolism and galactose metabolism pathway under salt stress

The metabolites content and gene expression levels were mapped to the sugar metabolism KEGG pathways, including starch and sucrose metabolism and galactose metabolism (Fig. 9A). In starch and sucrose metabolism, the sucrose content decreased at 6 h and increased at 12 h in BG, and dropped in MF, and it was higher in BG than that in MF (Fig. 9C). However, the amylose content increased at 6 h and decreased at 12 h in MF, but had no significant changes in BG, and it was significantly lower in BG than in MF (Fig. 9C). We identified four invertase (INV) among which *Iaqu.ptg000004l.g168* had a higher expression, five genes for alpha-amylase (AMY) among which four were higher, five genes trehalose 6-phosphate synthase (TPS) among which four exhibited high

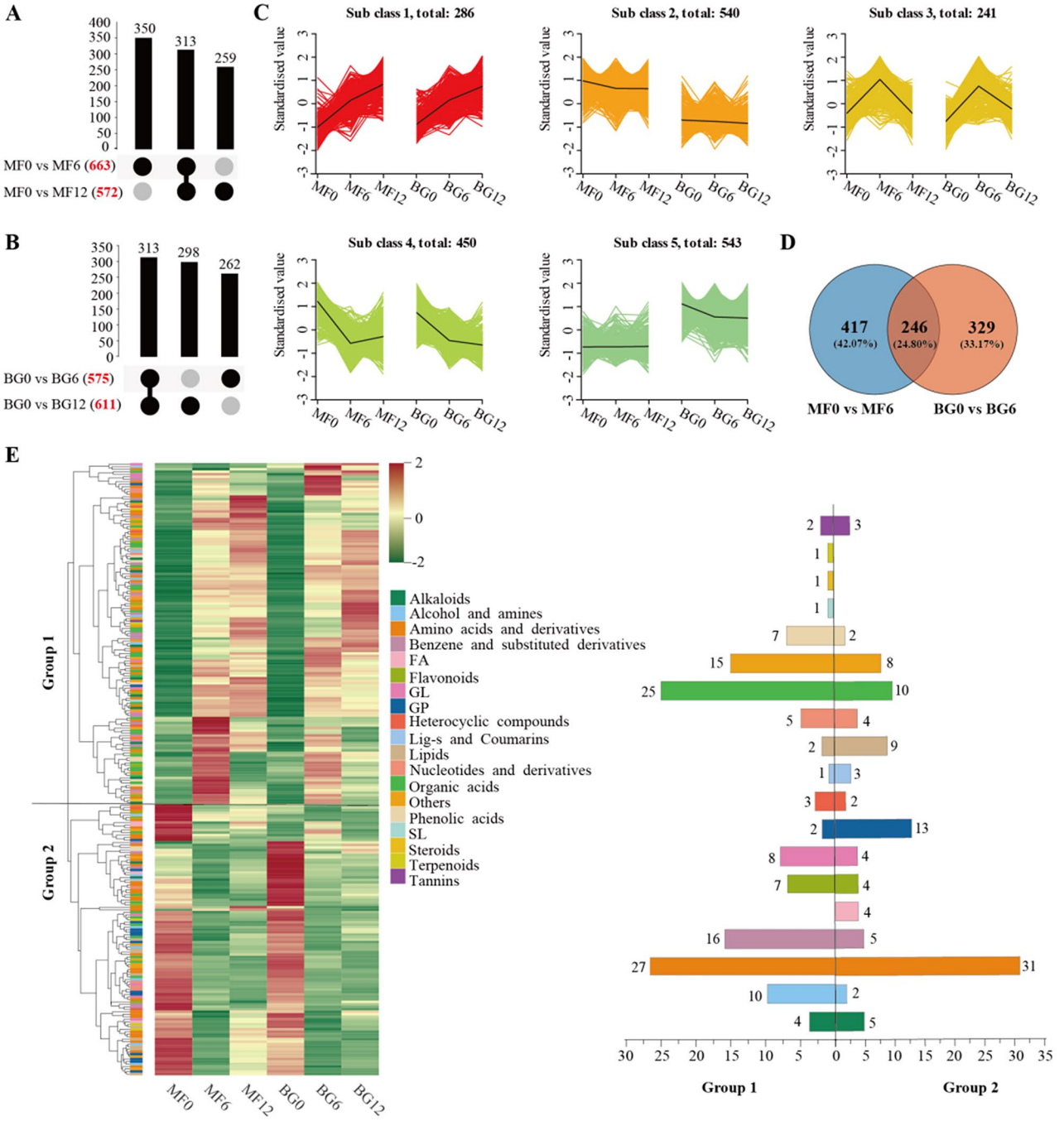

Fig. 8 Analysis of DAMs in water spinach roots under salt stress. The number of DAMs in MF (**A**) and BG (**B**). The column on the left indicates the number of DAMs in different pairwise comparisons. The column in the right indicates the overlapping and accession specific DAMs among the different comparisons. (**C**) K-MEAN analysis. (**D**) Venn diagram of DAMs in MF0 vs. MF6 and BG0 vs. BG6. (E) The heatmap analysis of 246 DAMs overlapped in MF0 vs. MF6 and BG0 vs. BG6. The two-way bar chart illustrates the quantity of DAMs of in each category in Group I and Group II

expression in BG at 6 h of salt treatment. Additionally, 17 genes encoding glucan endo-1,3-beta-glucosidase (GN) among which nine had higher expression, 11 genes for endoglucanase (EG) among which four showed higher expression in BG at 12 h ast-salt stress. Eight genes for trehalose 6-phosphate phosphatase (TPP) among which only *Iaqu.ptg000024l.g250* was up-regulated in both cultivars (Fig. 9B).

Sucrose produced in the cytoplasm is transferred to intermediate cells, where it is utilized for the synthesis of raffinose and stachyose by the enzymes raffinose synthetase (RFS) and stachyose synthase (STS) [33]. In galactose metabolism, the stachyose levels increased in BG and had

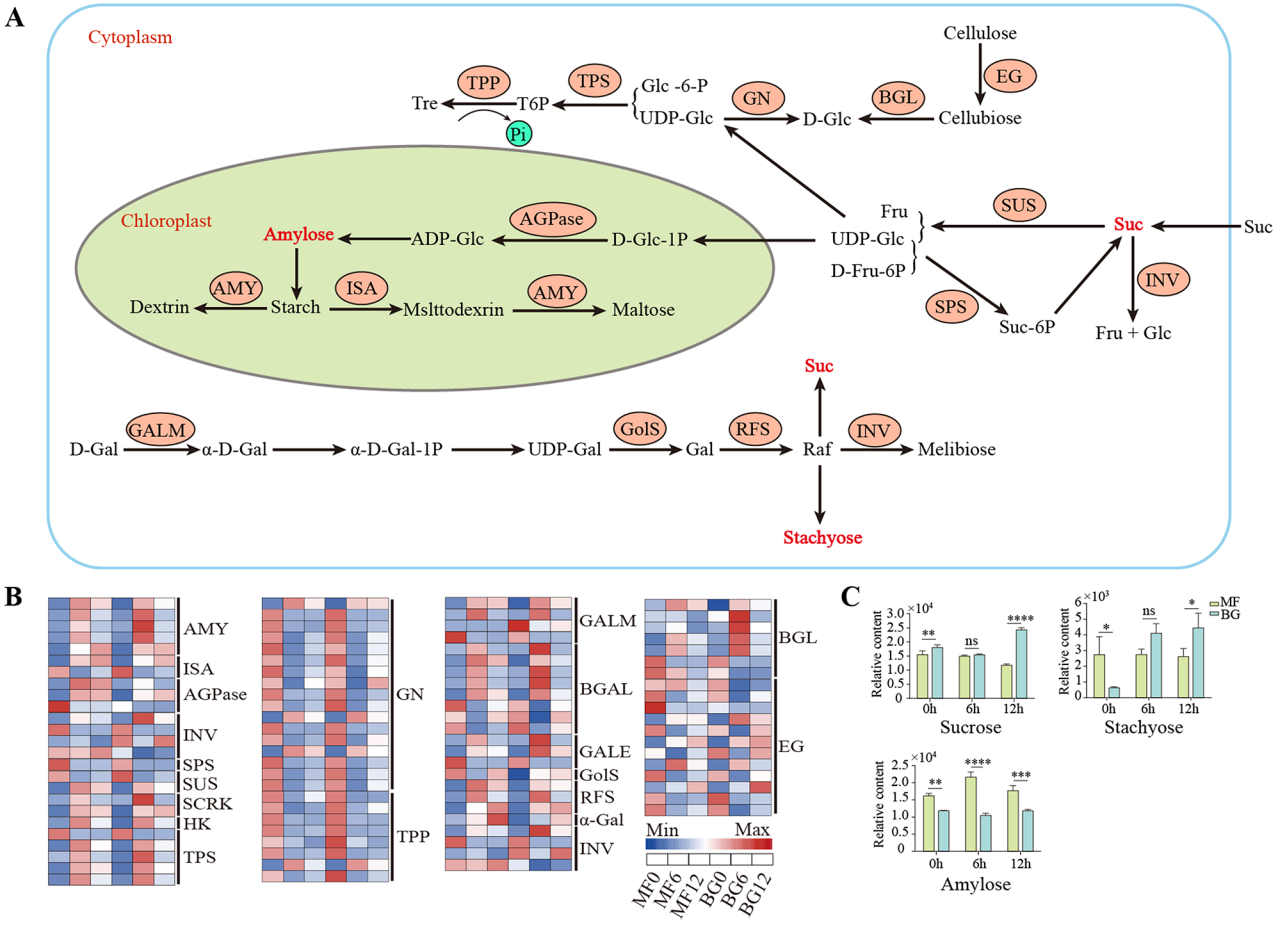

Fig. 9 Co-expression analysis of starch and sucrose metabolism and galactose metabolism. (**A**) Schematic diagram of the mechanism. (**B**) The heat maps displaying expression of DEGs. The heatmap colored in blue and yellow indicates metabolite accumulation. The heatmap colored in blue and pink indicates gene expression. Suc represented sucrose. (**C**) Changes in the content of key metabolites. AMY, alpha-amylase; ISA, isoamylase; AGPase, ADP-glucose pyrophosphorylase; INV, invertase; SPS, stachyose synthase; SUS, sucrose synthase; SCRK,; HK,; TPS, trehalose 6-phosphate synthase; GN, encoding glucan endo-1,3-beta-glucosidase; TPP, trehalose 6-phosphate phosphatase; GALM, aldose 1-epimerase; BGAL, beta-galactosidase; GALE, UDP-glucose 4-epimerase; GolS, galactinol synthase; RFS, raffinose synthetase; α-Gal, alpha-galactosidase; EG, endoglucanase

no significant changes in MF after salt stress, and it was significantly higher in BG than in MF upon salt stress (Fig. 9C). A total of 28 DEGs identified after salt stress. Three genes for raffinose synthase (RFS) had a higher degree of up-regulation expression, three genes for aldose 1-epimerase (GALM) among which two showed higher expression, eight genes for beta-galactosidase (BGAL) among which three had high expression, and three genes for UDP-glucose 4-epimerase (GALE) among which two exhibited higher expression in BG at 6 h of salt stress. One gene for alpha-galactosidase (α-Gal) was up-regulated in both species, but it had a stronger degree in BG. One galactinol synthase (GolS) was up-regulated in BG and down-regulated in MF (Fig. 9B). We elected eight genes from this two key metabolism (Table S2). After, performing qRT-PCR, we obtained a similar expression pattern for these genes as in RNA-seq data (Fig. S7 and S8).

Discussion

In this study, we selected the salt-tolerant cultivar BG and the salt-sensitive cultivar MF from a total of 59 germplasm resources. The phenotypic and physiological analysis indicated that, in comparison to MF, BG demonstrated a greater capacity for sustaining normal growth (Fig. 1A) and displayed a feature to accumulate higher levels of proline when exposed to salt stress (Fig. 1F). Proline acts as an osmotic agent, helping to regulate cellular osmotic pressure and improve the salt tolerance of plants [34]. In addition, salt-tolerant BG can also enhance its tolerance to salt stress by changing the transport capacity of cells to K^+ and Na^+ [35], regulating the sucrose and starch metabolism pathways [12], galactose synthesis pathway [36] hormone signaling pathway [37], and transcription factors regulating [38].

Under salt stress, excessive intracellular accumulation of Na^+ will affect the homeostasis of K^+ and then

interfere with the normal metabolic process of plants, and maintaining the balance of K^+ and Na^+ ions has become an important means for some salt-tolerant plants to adapt to salt stress [39]. In addition, maintaining the balance of these two ions relies on the activity of K^+ and Na^+ transport proteins [40]. In this study, compared with MF, BG not only significantly reduced the accumulation of Na^+, but also accumulated more K^+ after salt stress (Fig. 2A and B). Transcriptome analysis also revealed that the expression levels of genes *SOS2*, *CIPK8*, and *SCaBP8*, which are linked to Na^+ expulsion [39, 41], as well as *SKOR*, *ILK1*, and *KUP2*, which are related to K^+ uptake [42], were notably elevated in BG when exposed to salt stress. The findings indicated that BG facilitated the outflow of Na^+ and the inflow of K^+ to maintain ion homeostasis in response to salt stress (Fig. 10).

The accumulation of carbohydrates also plays an important role in the process of salt stress tolerance in plants. Sucrose can be used as an osmotic substance to stabilize the osmotic pressure of cells [33], and also regulate the complex and multi-layered regulation of root development and growth [43]. In this study, metabolomics results showed that the sucrose content of BG increased significantly after 12 h of salt treatment, while the sucrose content of MF gradually decreased with the extension of treatment time (Fig. 9C). At the same time, the expression levels of the three *AMY* genes used to degrade starch in BG were up-regulated and higher than those in MF (Fig. 9B), which may increase the content of glucose for sucrose synthesis. Raffinose family oligosaccharides (RFOs), such as stachyose, are osmoprotective agents (refs) that accumulate in response to abiotic stresses, and galactitol synthase (GolS) and raffinose synthase (RFS) are key enzymes involved in RFO biosynthesis [44]. In this study, metabolome analysis showed that compared with MF, stachyose in BG roots was significantly accumulated (Fig. 9C), and further transcriptome analysis showed that the expression of *Gols* and *RFS* in BG was significantly up-regulated at 6 h under salt stress, while the expression of *Gols* in MF was down-regulated at 6 h, and the expression of *RFS* was significantly lower than that of BG (Fig. 9B). These results indicated that BG would maintain cell osmotic pressure and ensure the normal growth and development of roots by degrading starch and increasing the accumulation of sucrose and stachyose after salt stress (Fig. 10).

Plant hormones not only regulate growth and development, but also play an important role in plant adaptation to salt stress [37]. For example, overexpression of gene *PR1* in the SA signaling pathway enhanced plant tolerance to salt stress [45]. This study showed that BG had higher *PR1* gene expression at 6 h compared with MF under salt stress. SA interacts with other hormones to regulate plant responses to salt stress. In wheat, for example, SA prevented the decline of auxin and cytokinin to promote growth to adapt salt tolerance in plants [46]. Compared with MF, the auxin-induced *SAUR* gene in BG was significantly expressed at 6 h of treatment

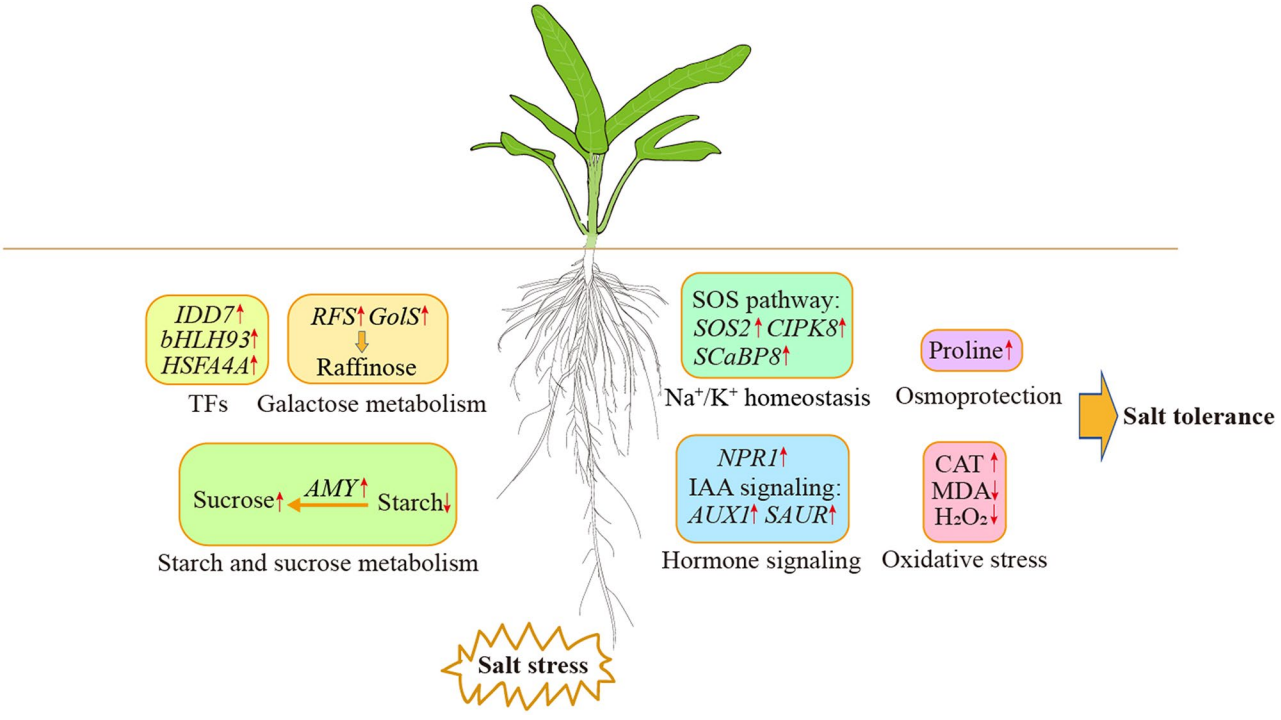

Fig. 10 Proposed model for molecular and physiological mechanisms underlying salt tolerance in water spinach

(Fig. 5). Studies have shown that transgenic *Arabidopsis* expressing wheat *TaSAUR75* exhibited significantly increased root length and elevated expression of stress-responsive genes under salt and drought stress compared to control plants [47]. Our phenotypic analyses revealed that the total root length, root volume, root surface area, and average root diameter of BG were significantly greater than those of MF following a 7-day salt treatment (Fig. 1B, C, D, E). These findings underscore the pivotal role of auxin in mediating BG's adaptive responses to salt stress. Sucrose provawides energy for root growth and coordinates root development by regulating auxin synthesis, transport, and signal transduction. For instance, sucrose affects the sensitivity of roots to auxin by regulating the expression of key components of auxin signaling pathway, such as ARF and Aux/IAA proteins [16]. Additionally, the bHLH transcription factor *SPATULA* in *Arabidopsis thaliana* regulates cell proliferation by modulating auxin accumulation or transport [48], further underscoring the interplay between bHLH transcription factors and auxin signaling in root development. In the present study, we identified a total of 45 bHLH transcription factors that were differentially expressed under salt stress conditions (Fig. S9). Notably, weighted gene co-expression network analysis (WGCNA) pinpointed *IabHLH093* as a critical transcription factor in BG (Fig. 11A). This suggests that *bHLH093* may play a central role in the regulatory network governing BG's salt stress tolerance, potentially through its influence on auxin-mediated pathways (Fig. 10).

Materials and methods

Plant materials and sampling

The seeds of 59 water spinach materials were purchased from seed companies in China. The names and sources of these water spinach are shown in Table S1. 'Baigeng Daye water spinach' (BG, salt-tolerant), purchased in Chenghai District, Shantou City, Chengqi Seed Trading Company, and 'Meifeng No.1 Liuye Banqingbai water spinach 318' (MF, salt-sensitive), purchased in Jieyang Agricultural Research Seed Industry Co., Ltd, were selected base on the salt-tolerant screening of 59 water spinach cultivars. Seeds were germinated in sterile Petri dishes (Φ = 150 mm) at 25 ℃ and then transferred to 50-hole discs in a climatic chamber under 25 ± 1 ℃ and 70% humidity at Guangdong Ocean University in Zhanjiang, Guangdong Province, China. After 2 weeks, the seedlings' roots were washed with distilled water to clean the substrate soil and transplanted into plastic pots filled with a 3.5 L 1/2 Hoagland solution. The optimal salt concentration for salt tolerance screening of water spinach was obtained from the pre-experiment, which was 150 mM NaCl. After 2 days, the plants' roots were placed in plastic pots with 0 mM NaCl (control group) and 150 mM NaCl (salt stress group) of 1/2 Hoagland solutions. Stir the salt daily solution to keep the NaCl concentration constant, and the salt solution was changed every 3 days with a pH of 6.0 ~ 6.5. For plant growth analysis, the seedlings were grown for 7 days under salinity conditions. For physiological, transcriptomic, and metabolomic analysis, root samples were collected at 0, 6, and 12 h post-salt-treatment, flash-frozen in liquid nitrogen, and stored at -80 ℃ until use.

Plant growth measurements

Leaf chlorophyll content (SPAD value) was measured by a chlorophyll meter (Konica Minolta, SPAD-502 Plus). Plant height (PH) and stem coarse (SC) were measured by straight ruler and vernier calipers respectively. Roots were rinsed with deionized water, and residual water was removed with filter paper. The fresh weight (FW) of a single plant, shoot fresh weight (SFW) and root fresh weight (RFW) were measured respectively. The ground and root were put into paper bags respectively, and the oven was 105 ℃ for 30 min and 80 ℃ for 48 h. The dry weight (DW) of a single plant, shoot dry weight (SDW) and root dry weight (RDW) were weighed with balance. The TRL, RSA, ARD, RV, and RTN were obtained by scanning using the Epson V700 (Seiko Epson Corp, Nagano, Japan) root scanner and analyzing using the WinRHIZO Root Scan Analysis system (WinRHIZO Regent Instruments Canada Inc, Montreal Canada). The water content (WC) and root shoot ratio (RSR) was calculated. The calculation formula is: WC = [(FW – DW) / FW]×100%; RSR = RFW (RDW) / SFW (SDW). The data corresponds to the mean of measurements on 15 biological replicates, and the standard error (SE) on these data.

Comprehensive salt-tolerance evaluations analysis

The values of growth and physiological indicators were converted into salt tolerance coefficients (STC). The PCA was performed on 19 traits' STC. The method of principal component weighting was first used to carry out a comprehensive salt-tolerance evaluation analysis of member function value (MFV). The systematic clustering method was used to classify the salt tolerance of the D value of the comprehensive salt tolerance evaluation. The calculation formula is shown in Supplementary Document 1.

Physiological indicators measurements

The measurements of superoxide dismutase (SOD) [49], POD [50], CAT [51], APX [52], proline levels [53], MDA levels [54], H_2O_2 concentrations [55], and the production rate of $O_2\bullet^-$ [56] in root tissue were conducted following the methods outlined in a previous study. The GR assay was performed using GR assay kit (A062-1-1) provided

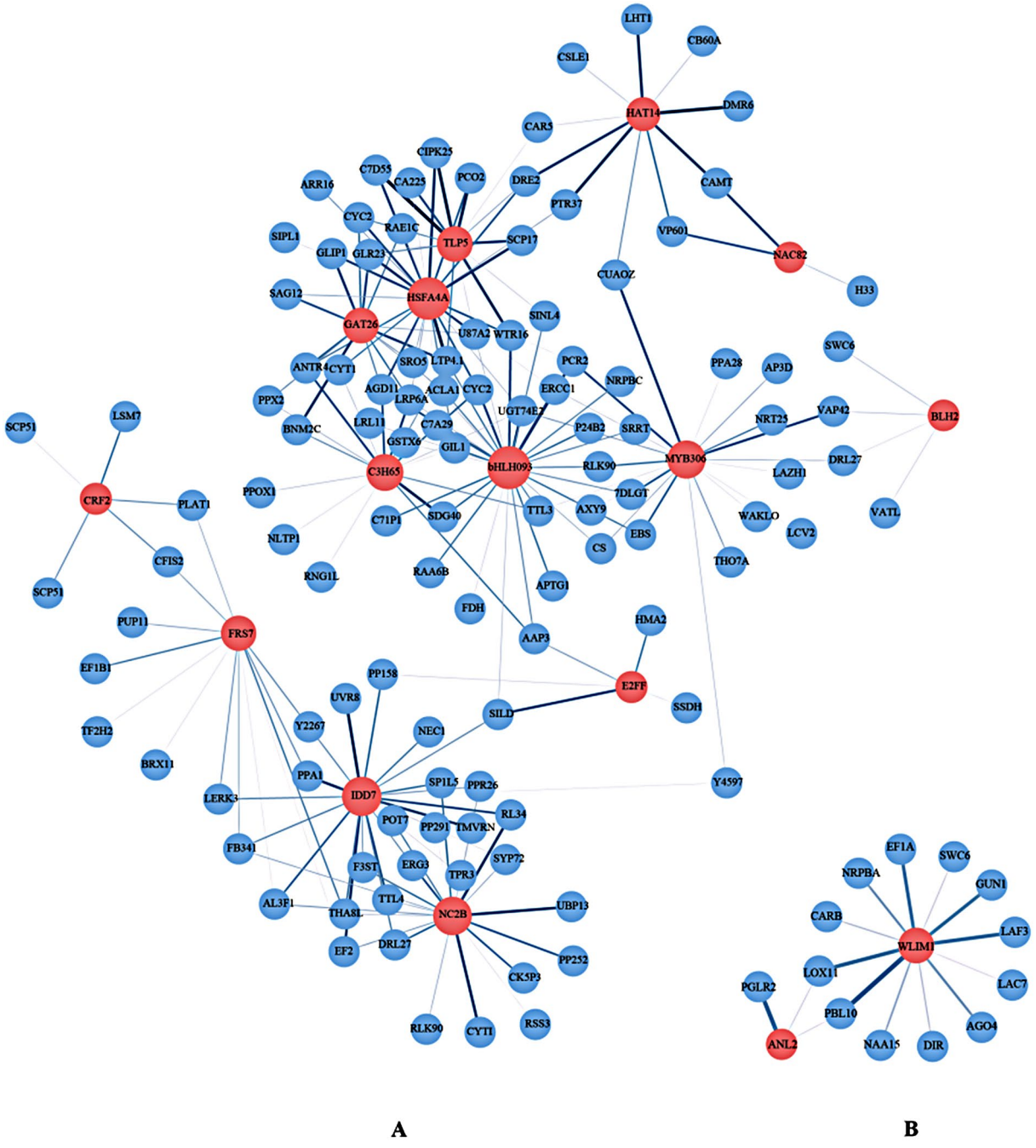

Fig. 11 The co-expression network of the transcription factors (TFs) and structural genes in the black (**A**), and cyan (**B**) modules. The red and blue circles represented transcript factors respectively. The size of red circles represented the quantities of interactions with structural genes. The dark-blue and light-blue lines represented the high and low degrees of interactions between TFs and structural genes respectively

by the Nanjing Institute of Bioengineering (Nanjing, China).

Accumulated mineral ions (Na^+, K^+, Ca^{2+}, and Mg^{2+})

All samples were weighed directly into 50 mL metal-free tubes, adding 2 mL of 69% nitric acid. The tubes were then placed on a digestion block (DigiPREP Jr., SCP-Science) at 120 ℃ until the solution was nearly evaporated. During this process, the tubes were gently swirled every 20 min. After cooling, 0.5 mL of H_2O_2 was added, and the samples were heated again for 30 min at 120 ℃. Once digestion was complete, the tubes were cooled to room temperature, and the volume was adjusted to 20 mL with ultrapure water. Aqueous calibration standards were created by diluting 1,000 mg/L ICP-MS standard solutions (Spex CertiPrep, America) with 10% nitric acid. Element

detection was performed using inductively coupled mass spectrometry (ICP-MS, NexION2000G, PerkinElmer, CA, USA), with element concentrations quantified through external calibration using aqueous standard solutions, and 103Rh was used as an internal standard.

RNA extraction, library construction, RNA sequencing, and data analysis

BG and MF were subjected to salt stress for 0, 6, and 12 h, and root tissues were collected for RNA sequencing (RNA-seq) analysis. Total RNA was isolated using the RNAprep Pure Plant kit from Tiangen (Beijing, China). The quality and integrity of the extracted RNA were assessed with the RNA Nano 6000 Assay Kit on the Bioanalyzer 2100 system from Agilent Technologies (CA, USA). Then, mRNA was isolated using the NEBNext Poly(A) mRNA Magnetic Isolation Module from NEB (E7490). The cDNA libraries were created using the NEBNext Ultra RNA Library Prep Kit and NEBNext Multiplex Oligos for Illumina (NEB, E7530) in accordance with the manufacturer's instructions.The cDNA libraries obtained from water spinach roots were sequenced using an Illumina HiSeq™ sequencing platform. The clean reads was obtained by using fastp to filter the original data, mainly to remove reads with adapters: when the N content in any sequencing reads exceeds 10% of the base number of the reads, remove the paired reads; when the number of low-quality ($Q <= 20$) bases in any sequencing reads contained in reads exceeds 50% of the bases of the reads, this paired reads will be removed. All subsequent analyses are based on clean reads. All clean reads were mapped to the *Ipomoea aquatica* Forsk. reference genome came from DDBJ (JARJNQ000000000) [31] with HISAT2 (version 2.0.4) at Metware Biotechnology Co., Ltd in Wuhan, China.

DEGs were identified using DESeq2 analysis with a fold change (FC) of at least 2 and a false discovery rate (FDR) of less than 0.01. he functional annotation of these DEGs was performed by consulting seven databases, which include GO (Gene Ontology), KEGG (Kyoto Encyclopedia of Genes and Genomes Ortholog database), KOG/COG (Clusters of Orthologous Groups of proteins), Nr (NCBI non-redundant protein sequences), Pfam (Protein family), and Swiss-Prot (a manually curated protein sequence database). Transcript sequence reads have been deposited in the SRA database with accession SRR29281936-SRR29281953.

DEGs with fragments per kilobase per million (FPKM) values exceeding 1 were selected. A Weighted Gene Co-Expression Network Analysis (WGCNA) was conducted using the WGCNA R package (version 1.68) [57]. The co-expression network was then visualized with Cytoscape 3.8.0.

Metabolite profiling and data analysis

Untargeted metabolomics analysis was conducted by Metware Biotechnology Co. Ltd. in Wuhan, China. The biological samples were initially freeze-dried and then pulverized into a fine powder. Next, 50 mg of the powder was dissolved in 1200 µL of cold 70% methanol that included an internal standard. The mixture was vortexed six times at 30-minute intervals, then centrifuged. The supernatant was filtered and kept for UPLC-MS/MS analysis.

The LC-MS system analytical parameters were set as follows: UPLC column was a Waters ACQUITY UPLC HSS T3 with a particle size of 1.8 µm and dimensions of 2.1 mm x 100 mm; the column temperature was maintained at 40 °C; the flow rate was 0.40 mL/min; the injection volume was 4 µL; and the solvent system consisted of water (0.1% formic acid) and acetonitrile (0.1% formic acid). Sample analysis utilized a gradient program that began with 95% solvent A and 5% solvent B. Over 5 min, a linear gradient was established to reach 35% A and 65% B, followed by a transition to 1% A and 99% B within 1 min, which was held for 1.5 min. Finally, the composition was reverted to 95% A and 5% B within 0.1 min and maintained for 2.4 min.

Unsupervised PCA was performed using the 'prcomp' function in R (www.r-project.org). HCA of the samples and metabolites was represented as heatmaps along with corresponding dendrograms. Simultaneously, PCC among the samples were calculated using the 'cor' function in R and were also displayed as heatmaps. Both HCA and PCC visualizations were created using the R package Complex Heatmap. DAMs were identified based on VIP (VIP > 1) and absolute Log2FC (|Log2FC| ≥ 1.0). VIP values were obtained from the OPLS-DA results, which included score plots and permutation plots, generated with the R package MetaboAnalystR. The data underwent log transformation (log_2) and mean centering prior to OPLS-DA. To prevent overfitting, a permutation test with 200 permutations was conducted.

Quantitative real-time PCR (qRT-PCR)

Total RNA was extracted from water spinach root samples using the Tiangen RNA Pure Plant kit (Tiangen, Beijing, China). The purity, concentration, and integrity of total RNA were measured by a NanoDrop 2000 spectrophotometer (Thermo Scientific, Wilmington, DE, USA). The synthesis of first-strand cDNA was performed using the *Evo M-MLV* Reverse Transcription Premixed Kit with gDNA Eraser (Acray Biotechnology Co., Ltd, Hunan, China). qPCR was carried out in a 20 µL reaction volume using the SYBR Gtrrn *Pro Taq* HS Premixed qPCR Kit II(Acray Biotechnology Co., Ltd, Hunan, China). The primer sequences of genes were listed (Table S2).

Data analysis

Microsoft Office 2022 (Microsoft, USA) was used for statistical analysis and data preprocessing. Analysis of variance (ANOVA) and the least significant difference (LSD) test were conducted using IBM SPSS Statistics 26.0 Statistics (SPSS Inc., Chicago, IL, USA). The HCA and PCC were computed using the ComplexHeatmap package in R. The PCA was conducted using the prcomp function in R (www.r-project.org). Graphs were generated using GraphPad Prism 8, Cytoscape 3.8.0, and Tbtools.

Supplementary Information

The online version contains supplementary material available at https://doi.org/10.1186/s12864-025-11409-z .

Supplementary Material 1

Acknowledgements
Not applicable.

Author contributions
Z. L: Methodology, Investigation, Data curation, and Writing-Original draft preparation. L. C: Investigation, Software, Validation. S. L: Investigation. G. L: Investigation. S. L: Investigation. D. X: Investigation. R. C: Methodology. F. F: Supervision. J. W and C. Z: Project administration, Conceptualization, Writing-Reviewing, and Editing. All authors read and approved the manuscript.

Funding
This work was funded by the National Natural Science Foundation of China (No. 32370359).

Data availability
Sequence data that support the findings of this study have been deposited in the National Center for Biotechnology Information with the primary accession code PRJNA1119567.

Declarations

Ethics approval and consent to participate
Not applicable.

Consent for publication
Not applicable.

Competing interests
The authors declare no competing interests.

Author details
[1]College of Coastal Agricultural Sciences, Guangdong Ocean University, Zhanjiang 524088, China
[2]Yangjiang Institute of Agricultural Sciences, Yangjiang Municipal Bureau of Agriculture and Rural Affairs, Yangjiang 529800, China
[3]South China Branch of National Saline-Alkali Tolerant Rice Technology Innovation Center Zhanjiang, Zhanjiang 524088, China

Received: 29 September 2024 / Accepted: 25 February 2025
Published online: 11 March 2025

References

1. Singh A. Soil salinity: A global threat to sustainable development. Soil use Manage. 2022;38(1):39–67.
2. Eswar D, Karuppusamy R, Chellamuthu S. Drivers of soil salinity and their correlation with climate change. Curr Opin Env Sust. 2021;50:310–8.
3. Hailu B, Mehari H. Impacts of soil salinity/sodicity on soil-Water relations and plant growth in dry land areas: A review. J Nat Sci Res. 2021;12(3):1–10.
4. Zaman M, Shahid SA, Heng L. Guideline for salinity assessment, mitigation and adaptation using nuclear and related techniques. Cham: Springer Nature; 2018.
5. Shabala S. Learning from halophytes: physiological basis and strategies to improve abiotic stress tolerance in crops. Ann Bot-London. 2013;112(7):1209–21.
6. Munns R, Tester M. Mechanisms of salinity tolerance. Annu Rev Plant Biol. 2008;59:651–81.
7. Liang W, Ma X, Wan P, Liu L. Plant salt-tolerance mechanism: A review. Biochem Bioph Res Co. 2018;495(1):286–91.
8. Hasanuzzaman M, Fujita M. Plant responses and tolerance to salt stress: physiological and molecular interventions. Int J Mol Sci. 2022;23(9):4810.
9. Benito B, Haro R, Amtmann A, Cuin TA, Dreyer I. The twins K + and Na + in plants. J Plant Physiol. 2014;171(9):723–31.
10. van Zelm E, Zhang Y, Testerink C. Salt tolerance mechanisms of plants. Annu Rev Plant Biol. 2020;71(1):403–33.
11. Waheed A, Zhuo L, Wang M, Hailiang X, Tong Z, Wang C, Aili A. Integrative mechanisms of plant salt tolerance: biological pathways, phytohormonal regulation, and technological innovations. Plant Stress. 2024;14:100652.
12. Dong S, Beckles DM. Dynamic changes in the starch-sugar interconversion within plant source and sink tissues promote a better abiotic stress response. J Plant Physiol. 2019;234:80–93.
13. Krasensky J, Jonak C. Drought, salt, and temperature stress-induced metabolic rearrangements and regulatory networks. J Exp Bot. 2012;63(4):1593–608.
14. Ruan Y, Jin Y, Yang Y, Li G, Boyer JS. Sugar input, metabolism, and signaling mediated by Invertase: roles in development, yield potential, and response to drought and heat. Mol Plant. 2010;3(6):942–55.
15. O'Hara LE, Paul MJ, Wingler A. How do sugars regulate plant growth and development? New insight into the role of trehalose-6-phosphate. Mol Plant. 2013;6(2):261–74.
16. Mishra BS, Sharma M, Laxmi A. Role of sugar and auxin crosstalk in plant growth and development. Physiol Plant 2022;174(1).
17. Ribba T, Garrido-Vargas F, O Brien JA. Auxin-mediated responses under salt stress: from developmental regulation to biotechnological applications. J Exp Bot. 2020;71(13):3843–53.
18. Teale WD, Paponov IA, Palme K. Auxin in action: signalling, transport and the control of plant growth and development. Nat Rev Mol Cell Biol. 2006;7(11):847–59.
19. Julkowska MM, Testerink C. Tuning plant signaling and growth to survive salt. Trends Plant Sci. 2015;20(9):586–94.
20. Ahanger MA, Aziz U, Alsahli AA, Alyemeni MN, Ahmad P. Influence of Exogenous Salicylic Acid and Nitric Oxide on Growth, Photosynthesis, and Ascorbate-Glutathione Cycle in Salt Stressed Vigna angularis. Biomolecules 2020;10(1):42.
21. Wang W, Zhao X, Li M, Huang L, Xu J, Zhang F, Cui Y, Fu B, Li Z. Complex molecular mechanisms underlying seedling salt tolerance in rice revealed by comparative transcriptome and metabolomic profiling. J Exp Bot. 2015;67(1):405–19.
22. Nawrot R, Barylski J, Lippmann R, Altschmied L, Mock H. Combination of transcriptomic and proteomic approaches helps to unravel the protein composition of Chelidonium majus L. milky Sap. Planta. 2016;244(5):1055–64.
23. Liu Y, Zheng J, Ge L, Tang H, Hu J, Li X, Wang X, Zhang Y, Shi Q. Integrated metabolomic and transcriptomic analyses reveal the roles of Alanine, aspartate and glutamate metabolism and glutathione metabolism in response to salt stress in tomato. Sci Hortic-Amsterdam. 2024;328:112911.
24. Xu Z, Chen X, Lu X, Zhao B, Yang Y, Liu J. Integrative analysis of transcriptome and metabolome reveal mechanism of tolerance to salt stress in oat (Avena sativa L). Plant Physiol Bioch. 2021;160:315–28.
25. Jin J, Wang J, Li K, Wang S, Qin J, Zhang G, Na X, Wang X, Bi Y. Integrated physiological, transcriptomic, and metabolomic analyses revealed molecular mechanism for salt resistance in soybean roots. Int J Mol Sci. 2021;22(23):12848.
26. Padilla YG, Gisbert-Mullor R, Bueso E, Zhang L, Forment J, Lucini L, López-Galarza S, Calatayud Á. New insights into short-term water stress tolerance through transcriptomic and metabolomic analyses on pepper roots. Plant Sci. 2023;333:111731.
27. Duong V, Nguyen T, Peka A, Bodrogi-Edit T, Hegedűs M, Kovacs T. Transfer and bioaccumulation of 210Po from soil to water spinach (Ipomoea aquatica Forrsk.) in Vietnam. J Environ Radioactiv. 2021;231:106554.

28. Gangopadhyay M, Das AK, Bandyopadhyay S, Das S. Water Spinach (Ipomoea aquatica Forsk.) Breeding. In: *Advances in Plant Breeding Strategies: Vegetable Crops.* Edited by J. M. JSMJ, vol. 10. Al-Khayri: Springer, Cham; 2021:183–215.
29. Dewanjee S, Swarnalata J, Niloy B, Tarun KD, Das S, Kalita J, Manna P. Edible leaf extract of Ipomoea aquatica Forssk. (Convolvulaceae) attenuates doxorubicin-induced liver injury via inhibiting oxidative impairment, MAPK activation and intrinsic pathway of apoptosis. Food Chem Toxicol. 2017;105:322–36.
30. Hao Y, Bao W, Li G, Gagoshidze Z, Shu H, Yang Z, Cheng S, Zhu G, Wang Z. The chromosome-based genome provides insights into the evolution in water spinach. Sci Hortic-Amsterdam. 2021;289:110501.
31. Jiang F, Wang S, Wang H, Xu D, Wang A, Yuan L, Fan W. Improved chromosome-level genome and annotation data for a leafy vegetable water spinach (Ipomoea aquatica). Sci Hortic-Amsterdam. 2023;320:112193.
32. Saeed Aljneibi RSA. Transcriptomic analysis of the glycophytic crop Ipomoea aquatica under salinity conditions compared to its wild halophyte relative Ipomoea pes-caprae. Al Ain City, emirate of Abu Dhabi. United Arab Emirates University; 2021.
33. Saddhe AA, Manuka R, Penna S. Plant sugars: homeostasis and transport under abiotic stress in plants. PHysiol Plant. 2021;171(4):739–55.
34. El Moukhtari A, Cabassa-Hourton C, Farissi M, Savouré A. How does proline treatment promote salt stress tolerance during crop plant development?? Front Plant Sci 2020;11.
35. Assaha DVM, Ueda A, Saneoka H, Al-Yahyai R, Yaish MW. The role of Na + and K + Transporters in salt stress adaptation in glycophytes. Front Physiol 2017;8.
36. Liu L, Wu X, Sun W, Yu X, Demura T, Li D, Zhuge Q. Galactinol synthase confers salt-stress tolerance by regulating the synthesis of galactinol and raffinose family oligosaccharides in Poplar. Ind Crop Prod. 2021;165:113432.
37. Yu Z, Duan X, Luo L, Dai S, Ding Z, Xia G. How plant hormones mediate salt stress responses. Trends Plant Sci. 2020;25(11):1117–30.
38. Rawat A, Völz R, Sheikh A, Mariappan KG, Kim S, Rayapuram N, Alwutayd KM, Alidrissi LK, Benhamed M, Blilou I et al. Salinity stress-induced phosphorylation of INDETERMINATE-DOMAIN 4 (IDD4) by MPK6 regulates plant growth adaptation in Arabidopsis. Front Plant Sci 2023;14.
39. Ali A, Petrov V, Yun D, Gechev T. Revisiting plant salt tolerance: novel components of the SOS pathway. Trends Plant Sci. 2023;28(9):1060–9.
40. Ji H, Pardo JM, Batelli G, Van Oosten MJ, Bressan RA, Li X. The salt overly sensitive (SOS) pathway: established and emerging roles. Mol Plant. 2013;6(2):275–86.
41. Yin X, Xia Y, Xie Q, Cao Y, Wang Z, Hao G, Song J, Zhou Y, Jiang X. The protein kinase complex CBL10–CIPK8–SOS1 functions in Arabidopsis to regulate salt tolerance. J Exp Bot. 2020;71(6):1801–14.
42. Li W, Xu G, Alli A, Yu L. Plant HAK/KUP/KT K + transporters: function and regulation. Semin Cell Dev Biol. 2018;74:133–41.
43. Göbel M, Fichtner F. Functions of sucrose and Trehalose 6-phosphate in controlling plant development. J Plant Physiol. 2023;291:154140.
44. ElSayed AI, Rafudeen MS, Golldack D, Weber A, Weber A. Physiological aspects of raffinose family oligosaccharides in plants: protection against abiotic stress. Plant Biol (Stuttgart Germany). 2014;16(1):1–8.
45. Chu N, Zhou J, Rott PC, Li J, Fu H, Huang M, Zhang H, Gao S. ScPR1 plays a positive role in the regulation of resistance to diverse stresses in sugarcane (Saccharum spp.) and Arabidopsis thaliana. Ind Crop Prod. 2022;180:114736.
46. Shakirova FM, Sakhabutdinova AR, Bezrukova MV, Fatkhutdinova RA, Fatkhutdinova DR. Changes in the hormonal status of wheat seedlings induced by salicylic acid and salinity. Plant Sci. 2003;164(3):317–22.
47. Guo Y, Jiang Q, Hu Z, Su X, Fan S, Zhang H. Function of the auxin-responsive gene TaSAUR75 under salt and drought stress. Crop J. 2018;2(6):181–90.
48. Makkena S, Lamb RS. The bHLH transcription factor SPATULA regulates root growth by controlling the size of the root meristem. Bmc Plant Biol. 2013;13(1):1.
49. Giannopolitis CN, Ries SK. Superoxide dismutases: I. Occurrence in higher plants. PLANT PHYSIOL. 1977;59(2):309–14.
50. Duarte-Vázquez MA, García-Almendárez BE, Regalado C, Whitaker JR. Purification and properties of a neutral peroxidase isozyme from turnip (Brassica Napus L. Var. Purple top white Globe) roots. J Agr Food Chem. 2001;49(9):4450–6.
51. Kair A, Omri G, Poljakoff-Mayber A. Peroxidase and catalase activity in leaves of Halimione portidacoides exposed to salinity. Physiol Plant. 1984;62:238–44.
52. Murcia MA, López-Ayerra B, Martinez-Tomé M, Vera AM, García-Carmona F. Evolution of ascorbic acid and peroxidase during industrial processing of broccoli. J Sci Food Agr. 2000;80(13):1882–6.
53. Wu W, Zhang Q, Ervin EH, Yang Z, Zhang X. Physiological mechanism of enhancing salt stress tolerance of perennial ryegrass by 24-Epibrassinolide. Front Plant Sci. 2017;8:1017.
54. Senthilkumar M, Amaresan N, Sankaranarayanan A. Estimation of malondialdehyde (MDA) by thiobarbituric acid (TBA) assay. In. New York, NY: Springer US; 2021:103–5.
55. Junglee S, Urban L, Sallanon H, Lopez-Lauri F. Optimized assay for hydrogen peroxide determination in plant tissue using potassium iodide. Am J Anal Chem. 2014;05(11):730–6.
56. Yang J, Cao Y, Zhang N. Spectrophotometric method for superoxide anion radical detection in a visible light (400–780 nm) system. Spectrochim Acta Part A Mol Biomol Spectrosc. 2020;239:118556.
57. Langfelder P, Horvath S. WGCNA: an R package for weighted correlation network analysis. BMC Bioinformatics. 2008;9(1):559.

Publisher's note